Journal of Photochemistry and Photobiology 18 (2023) 100212

Contents lists available at ScienceDirect

Journal of Photochemistry and Photobiology

journal homepage: www.sciencedirect.com/journal/journal-of-photochemistry-and-photobiology

Synthesis of $CuInS_2$ nanoparticles and application in the photocatalytic degradation of tetracycline

Damian C. Onwudiwe [a,b,*], Opeyemi A. Oyewo [c], Naledi H. Seheri [a,b], Mathato P. Motaung [b], Seshibe S Makgato [c], Sarah C. Motshekga [c]

[a] Department of Chemistry, School of Physical and Chemical Sciences, Faculty of Natural and Agricultural Sciences, North-West University, Mafikeng Campus, Private Bag X2046, Mmabatho 2735, South Africa
[b] Material Science Innovation and Modelling (MaSIM) Research Focus Area, Faculty of Agriculture, Science and Technology, North-West University (Mafikeng Campus), Private Bag X2046, Mmabatho, South Africa
[c] Department of Chemical Engineering, College of Science, Engineering and Technology, University of South Africa, South Africa

ARTICLE INFO

Keywords:
Microwave
Tetracycline
Ternary metal sulphide
Photo-degradation

ABSTRACT

A lot of effort has been given to the development of nontoxic ternary semiconductor nanoparticles that could act as photocatalyst NIR-I (750–850 nm) or NIR-II (1000–1400 nm) optical windows. This is due to their good stability, high optical absorption coefficient, and desirable band gap that absorbs well within the solar spectrum. $CuInS_2$ is one of the ternary sulphide semiconductors, which has been considered to be a highly promising photocatalyst. The properties are attributed to its high optical absorption coefficient. In this study, copper indium sulphide ($CuInS_2$) nanoparticles were synthesized by a microwave irradiation route using copper(II) bis (*N*-methyl-*N*-ethanol dithiocarbamate) and In(III) tris (*N*-methyl-*N*-ethanol dithiocarbamate) as a precursor complexes. The copper(II) complex was varied in two different ratios (3:1 and 2:1) to determine the best synthesis regime. Then, the effect of the varying ratios on the crystalline structure, morphology, and optical properties of the $CuInS_2$ was studied by using X-ray diffraction (XRD), scanning and transmission electron microscopy (SEM and TEM), and absorption spectroscopy. The microscopic analyses revealed that the $CuInS_2$ nanoparticles have similar spherical grain-like shapes whose sizes range between 10.3–50.1 nm. The increase in the concentration of copper(II) complex also altered the band gap energy, given 2.87 and 1.61 eV for $CuInS_2$(3:1) and $CuInS_2$(2:1) respectively. The photocatalytic activities of the nanoparticles were determined for the degradation of Tetracycline (TC) under visible light irradiation. The effects of process parameters such as photocatalyst dosage and initial concentration of TC were investigated to establish the optimal performance of the $CuInS_2$ nanoparticles. The experimental data showed a higher TC degradation percentage for $CuInS_2$(2:1) (95 %) compared to $CuInS_2$(3:1) (90 %), indicating its high potential as a photocatalyst for the degradation of TC in aqueous solution.

1. Introduction

Antibiotics are one of the most common and widely consumed drugs in the pharmaceutical industry [1]. Their global daily consumption was recorded to increase up to 65 % in a 15-year period [2]. China, for example, consumes up to 180,000 tons per annum of antibiotics for both human and agricultural purposes [3]. Tetracycline (TC) as a model antibiotic has been reported to be the most used antibiotic drug in the world. The products can also be classified as oxytetracycline and chlortetracycline, with their basic structural ring system composed of various hydroxyl, methyl, keto, and dimethylamino functional groups [4].

Despite its importance and effectiveness, the abuse of TC could be carcinogenic, and depressive to bone growth, besides the other common side effects such as nausea, constant headache, diarrhoea, continuous vomiting, loss of appetite, black hairy tongue, throat and mouth sores, dizziness, or rectal discomfort [5]. Tetracycline may also cause azotemia, hyperphosphatemia, acidosis, and could also increase blood urea nitrogen (BUN) and Fanconi syndrome in some patients. According to Chen et al., [6], TC are typical emerging contaminants (ECs) that are regarded as the most concerning global environmental threats to humans, aquatic, and terrestrial lives due to the frequency of their

* Corresponding author.
E-mail address: Damian.Onwudiwe@nwu.ac.za (D.C. Onwudiwe).

https://doi.org/10.1016/j.jpap.2023.100212

Available online 21 October 2023

occurrence in water bodies.

Tetracycline has been removed from water by different techniques such as adsorption [7], membrane technology [8], coagulation-sedimentation [9], and photocatalysis [10]. Amongst these techniques, photocatalysis has been reported as a promising technology for the effective removal of TC from water, owing to the ability of the process to completely degrade the organic pollutant into its non-toxic products. In addition, it is considered sustainable and cost-efficient due to its utilization of green technology [11,12]. Metal oxide semiconductors, such as TiO_2, SnO_2, and ZnO_2 have been used as photocatalysts for the degradation of TC in wastewater [11,13]. However, the poor utilization of visible light due to their large band gap energies is a major drawback. In addition, binary metal sulphides are visible–light driven photocatalysts with narrower band gap energies compared to those of the metal oxides, making it possible to maximally utilize solar energy [14].

Ternary metal sulphide–based photocatalysts have received research attention lately, because of their long–term stability, good thermal property, and a very large absorption coefficient over a wide spectral range [15,16]. Photocatalysts such as MIn_2S_4 [17], $Znln_2S_4$ [18], ZnCuCdS [12], and $CuInS_2$ [11] have a large specific surface area which possesses more active sites for the favourable transport of electrons and holes to the surface of the photocatalysts for photocatalytic reactions. This is because ternary metal sulphides nanoparticles possess relatively smaller band gaps, which in turn promotes the utilization of visible light directly.

Copper indium sulphide is one of the interesting ternary metal sulphides with a wide range of applications including photocatalysis [19,20]. Its conduction band is usually constructed from the 5 s orbital of In and its valence band consists of the 3p orbitals of S [21]; thus, results in a narrower band gap energy between 1.53 to 2.4 eV. The photocatalytic activity of $CuInS_2$ has been explored in the degradation of organic pollutants [22], nitrate ions reduction [23], and dye degradation [24]. However, their synthesis route property plays a significant role in their efficiency. Different methods of synthesis such as hydro/solvothermal, solvothermal, and microwave heating have been adopted for the preparation of $CuInS_2$[25,26].. However, the microwave irradiation method is less complicated, efficient, eco-friendly, and cost-effective amongst others, and has been reported for the synthesis of ternary nanoparticles [27].

In this study, we report the microwave irradiation method of synthesizing $CuInS_2$ nanoparticles using two precursor compounds: copper (II) bis (*N*-methyl-*N*-ethanol dithiocarbamate complex and In(III)tris (*N*-methyl-*N*-ethanol dithiocarbamate), in two different ratios. The choice of dithiocarbamates as precursor compounds compared to other related compounds is based on ease of synthesis under laboratory conditions, the ability to form stable compounds than several complexes, and the clean decomposition profile that leads to the corresponding metal sulphide [28] The $CuInS_2$ nanoparticles were characterized to establish the physiochemical properties using structural, spectroscopic, and morphological techniques. The photocatalytic degradation activities of the as-synthesized $CuInS_2$ nanoparticles were investigated using TC. The key operating parameters, such as photocatalyst dosage and initial TC concentration were also studied to establish the performance of the $CuInS_2$ nanoparticles. To the best knowledge of the authors, this report presents one of the pioneering studies involving a facile route to $CuInS_2$ via microwave irradiation of precursor compounds.

2. Experimental

2.1. Synthesis of copper indium sulphide nanoparticles using microwave-assisted method

All the reagents used are of analytical grade. Microwave irradiation synthesis of CuInS nanoparticles was carried out following an earlier reported procedure [29]. A mixture of copper(II) bis (*N*-methyl-*N*-ethanol dithiocarbamate complex (0.06 mmol) and In(III) tris (*N*-methyl-*N*-ethanol dithiocarbamate) complex (0.02 mmol) were dispensed in 30 mL ethylene glycol and sonicated for 10 min at 40 °C. Thereafter, the solution was transferred into a Teflon-lined microwave (Multiwave 3000 microwave sample system, Anton Paar, Synthos) sample holder and left for the reaction to proceed by cyclic microwave radiation at 800 W for 5 min. After the reaction, the precipitates were washed with ethanol and air-dried. This procedure was repeated using copper(II) bis (*N*-methyl-*N*-ethanol dithiocarbamate complex (0.04 mmol) and In(III) tris (*N*-methyl = *N*-ethanol dithiocarbamate) complex (0.02 mmol) to afford CuInS nanoparticles denoted as $CuInS_2$(3:1) and $CuInS_2$(2:1) respectively.

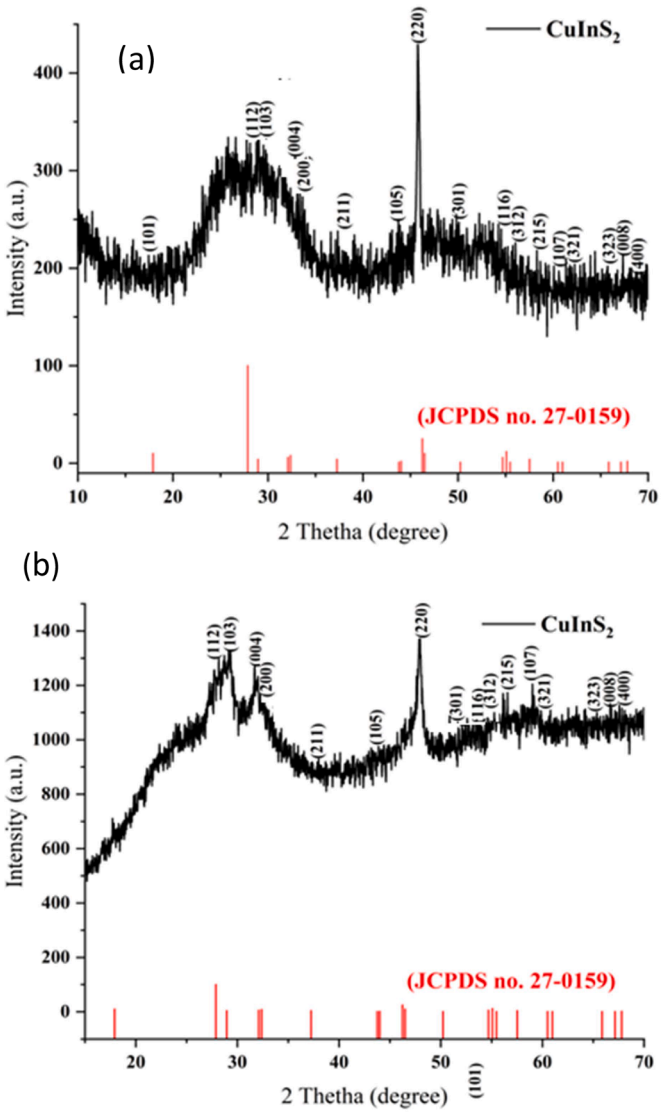

Fig. 1. Powder XRD patterns of (a) $CuInS_2$(3:1) and (b) $CuInS_2$(2:1) nanoparticles obtained using copper(II) bis(*N*-methyl-*N*-ethanol dithiocarbamate) and indium(III) tris(*N*-methyl-*N*-ethanol dithiocarbamateas precursor complexes.

2.2. Characterization of the prepared samples

Absorption measurements were carried out using Varian UV–vis spectrophotometer. Photoluminescence (PL) spectra were recorded on a Perkin Elmer LS 45 Fluorimeter. Diffraction patterns of the samples were obtained on Bruker D8 Advanced XRD instrument, and the patterns obtained were compared to the standard JCPDS database. The

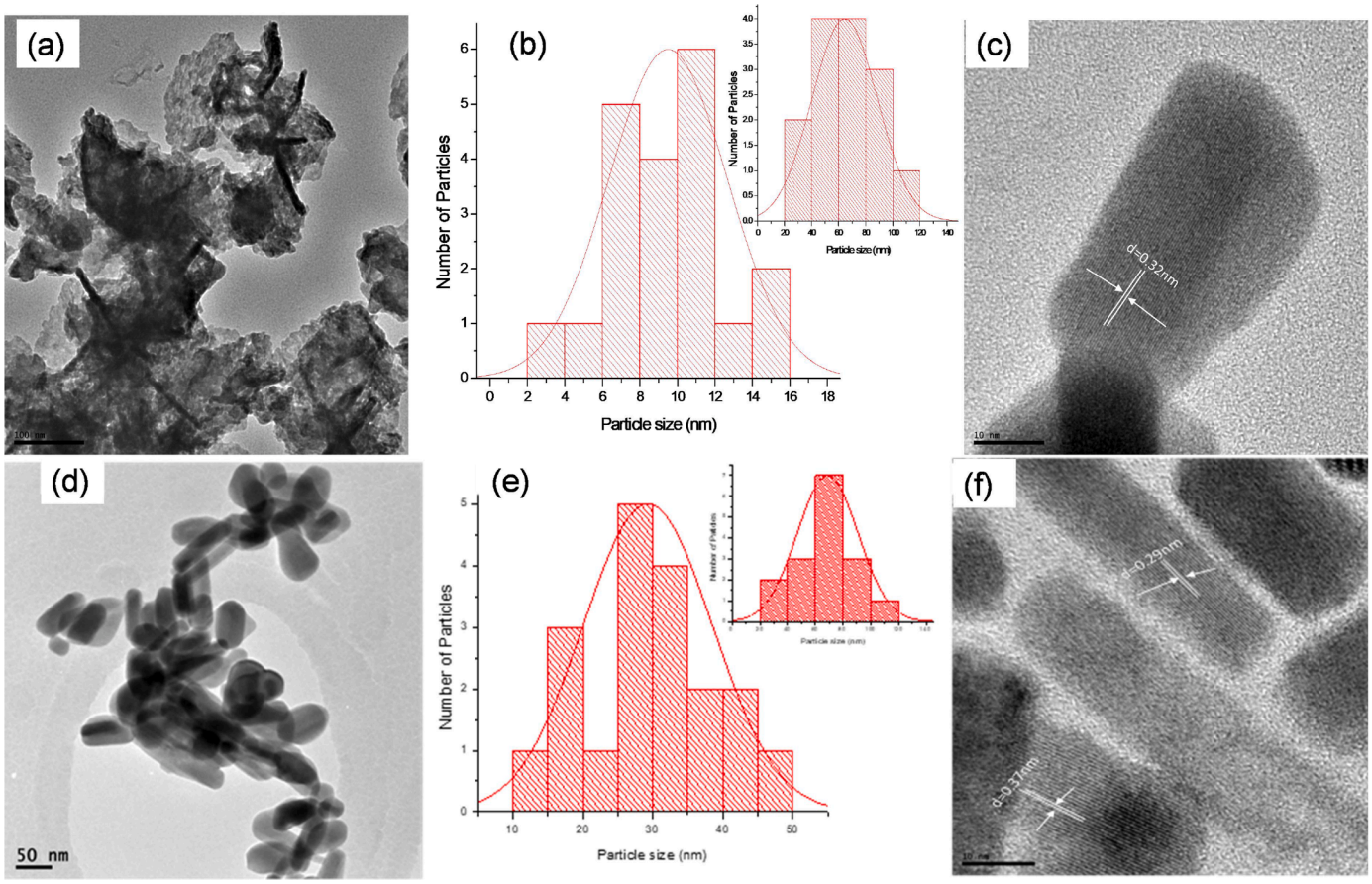

Fig. 2. (a) TEM, (b) size distribution histograms, and (c) HRTEM micrographs of $CuInS_2$(3:1) nanoparticles. (d) TEM, (e) size distribution histograms, and (f) HRTEM micrographs of $CuInS_2$(2:1) nanoparticles.

morphology of the samples was analysed using a JEOL 6400F Field Emission SEM at 5 kV and Hitachi HF–2000 TEM at 200 kV.

2.3. Photocatalytic activity of $cuins_2$(3:1) and $cuins_2$(2:1) nanoparticles

The photocatalytic activities of $CuInS_2$(3:1) and $CuInS_2$(2:1) nanoparticles were evaluated on the degradation of TC under visible light irradiation using a 25–W high-pressure mercury lamp of wavelength of 365 nm. The process parameters such as the initial concentrations of TC and catalyst loading were also investigated on the photocatalytic performances. A known amount of the nanoparticles was dispersed separately in 1000 mL of TC solution with initial concentrations in the range of 20–120 mg/L to investigate the influence of initial TC concentration on photocatalytic performance. In each experiment, the mixture of TC and catalysts was magnetically stirred thoroughly in the dark for 1 h to achieve an adsorption–desorption equilibrium prior to the irradiation. Thereafter, the solution was irradiated and at specific time intervals, 5 mL aliquots were sampled and centrifuged to remove the spent photocatalyst, and the concentration of residual TC in the supernatant solutions was quantified using a UV–vis spectrophotometer. The same experiment was repeated to determine the optimal dosage for the initial concentration of TC. The photo-degradation efficiency was estimated using the following equation:

$$\text{Degradation yield } \% = \frac{C_o - C_t}{C_o} \times 100 \quad (1)$$

where C_0 is the initial concentration of TC (mg/L) and C_t is the concentration of TC (mg/L) at time t.

3. Results and discussion

3.1. X-ray diffraction (XRD) analysis

The XRD pattern of $CuInS_2$(3:1) and $CuInS_2$(2:1) are shown in Figs. 1a and b. The XRD pattern of the $CuInS_2$(3:1) shows the pronounced peaks at 28.9, 31.3, and 45.7° that could be assigned to the (1 0 1), (1 0 2), and (1 1 0) planes of the orthorhombic $CuInS_2$ structure. While the XRD pattern of the $CuInS_2$(2:1) shows pronounced peaks at 29.1, 31.6, and 47.8°, which also corresponded to the (1 0 1), (1 0 2), and (1 1 0) planes. The diffraction peaks could be indexed to the crystal phase of wurtzite $CuInS_2$ according to the JCPDS card no. 27–0159 [30]. There were no peaks that could be attributed to CuS, Cu_2S, In_2S_3 or β-In_2S_3 detected in both XRD patterns, and this was indicative that the chosen precursor ratios promoted the formation of single-phase ternary nanoparticles. The lattice parameters were $a = 3.89$ Å and $c = 6.44$ Å and with space group P63mc [31]. The average crystallite sizes estimated using the Debye-Scherer formula gave 32.6 and 35.4 nm for the $CuInS_2$(3:1) and $CuInS_2$(2:1), respectively. Similar results have been reported in the XRD pattern of copper-based catalysts [32–34].

3.2. Morphology studies by electron microscopy

The internal morphologies of both as-synthesized $CuInS_2$ nanocomposites are presented in Fig. 2. The TEM micrograph of $CuInS_2$(3:1) displayed needle-like shapes which were embedded within some agglomerated sheets (Fig 2a). The agglomeration might be due to the high reaction and precursor decomposition which could be due to the microwave irradiation [35]. Initially, Cu^{2+} ions are converted to Cu^{+} through the solvent, ethylene glycol, acting as a reducing agent [36].

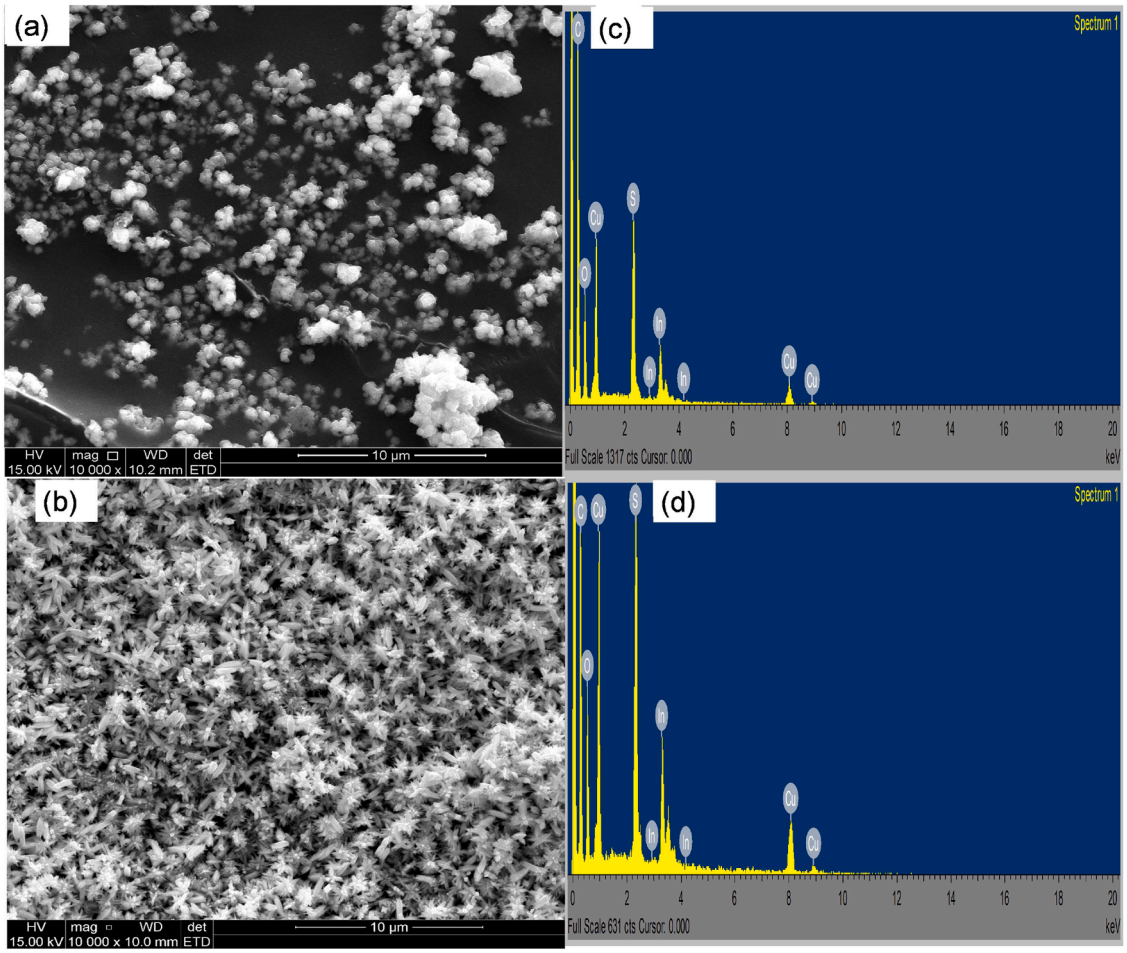

Fig. 3. (a) SEM images of (a) $CuInS_2$(3:1), (b) $CuInS_2$(2:1), (c) EDX micrograph of (c) $CuInS_2$(3:1) and (d) $CuInS_2$(2:1) nanoparticles.

Subsequently, the Cu^+ ions then react with In^{3+} and S^{2-} ions to produce $CuInS_2$ nuclei, which grow under high temperatures, similar to an earlier reported process by Hosseinpour-Mashkani *et al.* [36]. Fig. 2b shows that the particle sizes were in the range of 2.12–15.7 nm, with an average diameter and length of 9.71 nm and 78.2 nm, respectively. The HRTEM image presented in Fig. 2c shows that the low magnification needle-like shapes were rod-like crystals at high resolution with fringes whose lattice spacing of 0.32 nm aligns with the (1 1 2) plane of $CuInS_2$ [37].

Fig. 2(d) presents the TEM image of $CuInS_2$ (2:1), which showed nanorods with slight agglomeration. The observed agglomeration may be ascribed to the high surface activity of the wurtzite $CuInS_2$ nanoparticles [31]. The size distribution histogram showed nanoparticles whose sizes range between 10.3–50.1 nm; with a mean diameter of 31.3 nm and an average length of 72.7 nm as presented in Fig. 2(b). The HRTEM shown in Fig. 2f shows rod-shape with lattice fringes, whose distance of 0.29 and 0.37 nm were orientated in different directions and corresponded to the (1 0 1) and (1 0 3) planes, respectively, of the wurtzite $CuInS_2$ structure [38].

Fig. 3 shows the SEM image of $CuInS_2$ with nanoparticles and noticeable agglomerates. The micrograph of $CuInS_2$(3:1) presented in Fig. 3a displays spherical grain-like structures formed from agglomerated short nanorods. Fig. 3b showed interlocked spindle-like particles whose morphology was distinctly different from the observed morphology of $CuInS_2$(2:1). The observed morphology was similar to $CuInS_2$ nanoparticles reported by Long et al. [39] using ultrasonic process, which showed how different methods of preparation could affect the final morphology of the products obtained.

The elemental composition of both nanoparticles (Figs 3c and d) showed the peaks for carbon, copper, sulphur, oxygen, and indium corresponding to $CuInS_2$.

3.3. Absorbence studies

The UV–vis spectra show absorption peaks in the visible region at 434 and 441 nm, respectively for $CuInS_2$(3:1) and $CuInS_2$(2:1) (Figs 4a and b). In addition to the absorption in the visible region, $CuInS_2$(2:1) also displayed a broad absorption peak in the near-infrared region as presented in Fig. 4b. The estimated band gap energies from the Tauc plot were found to be 2.87 and 1.61 eV, respectively for $CuInS_2$(3:1) and $CuInS_2$(2:1) as shown in Figs 4c and d, which indicated a red-shift relative to the bulk $CuInS_2$ (1.55 eV) [40]. The observed red-shift in the bandgap energy conforms to the quantum confinement effect. In addition, the increase in the band gap is associated with a decrease in crystallite size [41]. Similar to related reports on $CuInS_2$ nanoparticles, the optical absorption blue-shift is related to the quantum confinement effects. However, $CuInS_2$(2:1) showed a slight difference compared to the bulk material, this may be ascribed to the structural difference of the nanoparticle.

3.4. Photocatalytic degradation of tc using $cuins_2$(3:1) and $cuins_2$(3:1) nanoparticles

The catalytic activity of the synthesized $CuInS_2$(2:1) and $CuInS_2$(3:1) nanoparticles was evaluated on the photodegradation of TC, under the visible light irradiation as presented in Figs. 5a and b. Both $CuInS_2$(3:1) and $CuInS_2$(2:1) showed weak TC photodegradation ability at 0 min before the irradiation with light. Similar degradation patterns were observed for both $CuInS_2$(2:1) and $CuInS_2$(3:1) nanoparticles. The two

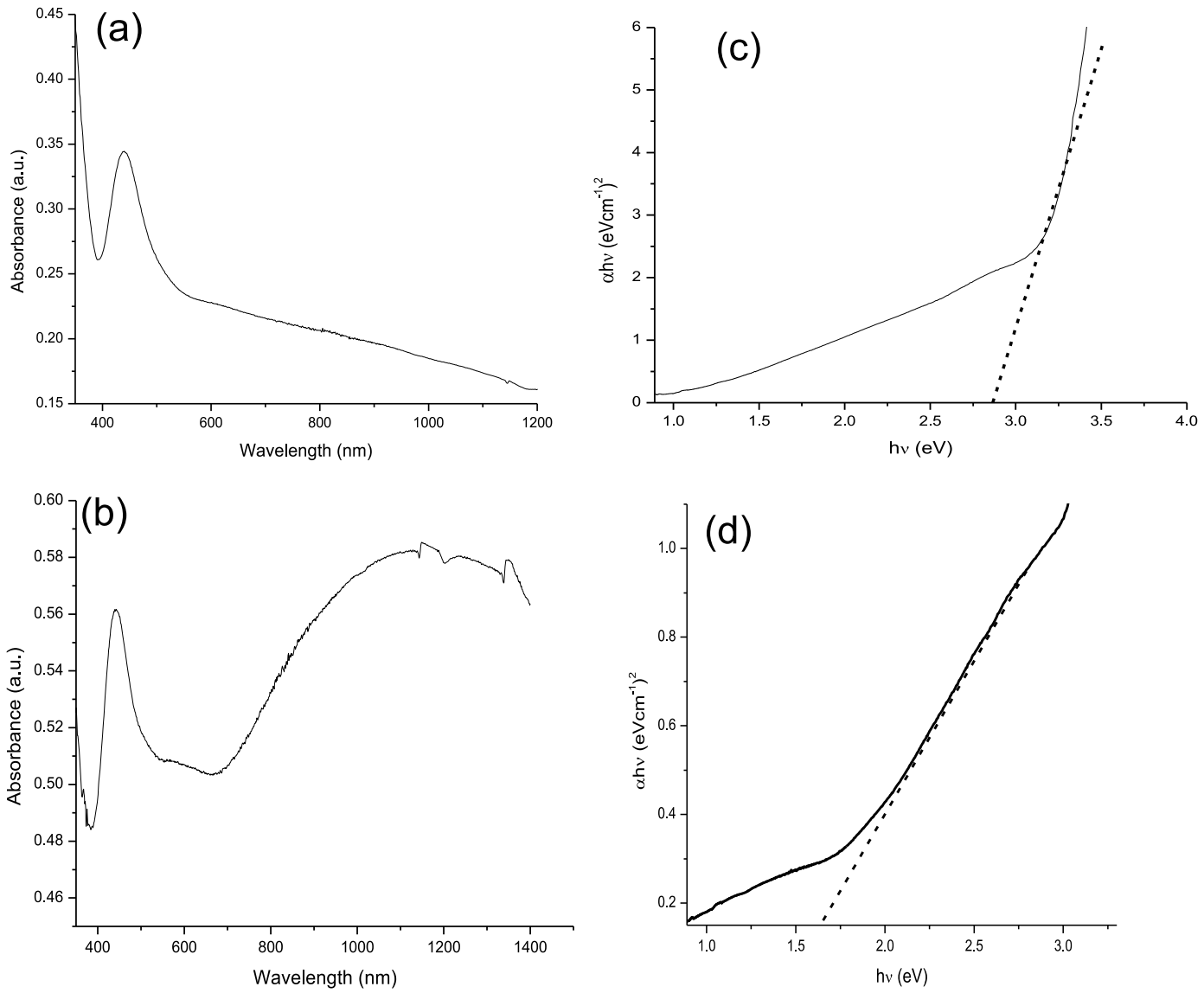

Fig. 4. UV–vis-NIR and corresponding Tauc plot of $CuInS_2$(3:1) (a,b) and $CuInS_2$(1:1) (c,d) nanoparticles.

absorption bands at approx. 275 and 360 nm are ascribed to the double-bond structures of two carbonyl groups and enolic groups, respectively [42]. A sequential decrease in the intensity of these absorption peaks as well as a slight shift towards higher wavelengths was observed as the irradiation time increased. After visible light irradiation for 90 min, the degradation rates of TC by both nanoparticles, $CuInS_2$(2:1) and $CuInS_2$(3:1), increased to 95 % and 91 %, respectively, which may be due to their electronic structure [43]. $CuInS_2$(2:1) exhibited better photocatalytic activity compared to the $CuInS_2$(3:1) and could be attributed to the higher absorption properties of the $CuInS_2$(2:1). Nevertheless, the degradation efficiency obtained for $CuInS_2$(3:1) is highly comparable to other catalysts reported in the literature [43,44]. Hence, the CuInS2(2:1) nanoparticles were used for the subsequent degradation experiments in this study.

3.4.1. *Effect of catalysts ($CuInS_2$(2:1)) loading*

The influence of catalyst dosage between 10 and 125 mg/L concentration on the removal of 20 mg/L solution of TC was studied under visible light. Fig. 6 shows that negligible changes occurred in the concentration of TC before the introduction of $CuInS_2$. The photodegradation of TC increased with an increase in the amount of nanoparticles until 125 mg/L after 90 min at pH = 4. Thereafter, little or no degradation of TC was observed with a further increase in $CuInS_2$. Therefore, the optimal or equilibrium dosage concentration was determined and found to be 125 mg/L, which resulted in almost complete degradation of TC. Hence, the TC degradation efficiency within 90 min of reaction was elevated from 37.8 % to 98.1 % when the $CuInS_2$ dosage increased from 10 to 125 mg. This observation could be ascribed to the increase in the availability of numerous photo-induced active species which increased the interaction of the catalyst with the TC molecules effectively [45]. These results were in accordance with some earlier reported studies involving the degradation performances of copper-based photocatalysts [42,46].

3.4.2. *Effect of initial concentration of TC*

As presented in Fig. 7, the efficiency of different $CuInS_2$ was investigated using different initial concentrations of TC. It could be observed that the removal efficiency of the photocatalyst decreased with an increase in the initial TC concentrations from 20 to 120 mg/L under the visible light after 90 min reaction, which reflected lower removal efficiency at higher TC concentrations. This is an indication that the TC degradation rate decreases with an increase in the initial concentration of TC. This phenomenon could be attributed to the decrease in the formation of hydroxyl radicals at higher TC concentrations, as more TC ions

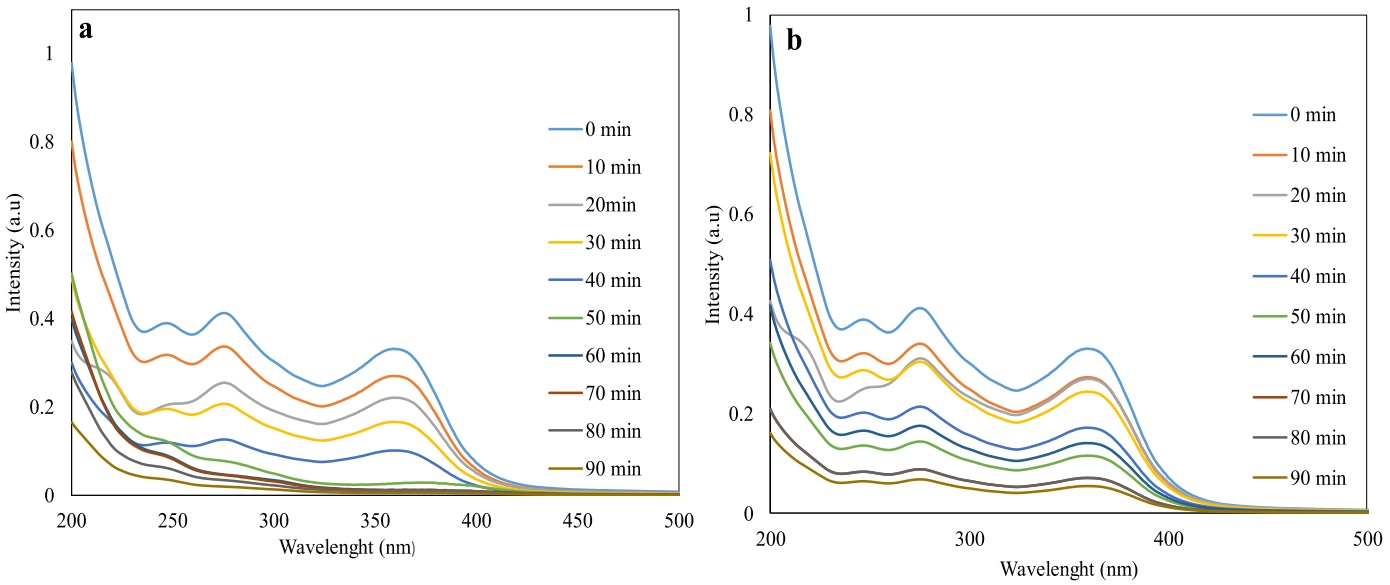

Fig. 5. Photocatalytic degradation of tetracycline under visible light irradiation using (a) $CuInS_2$(2:1) and (b) $CuInS_2$(3:1) nanoparticles.

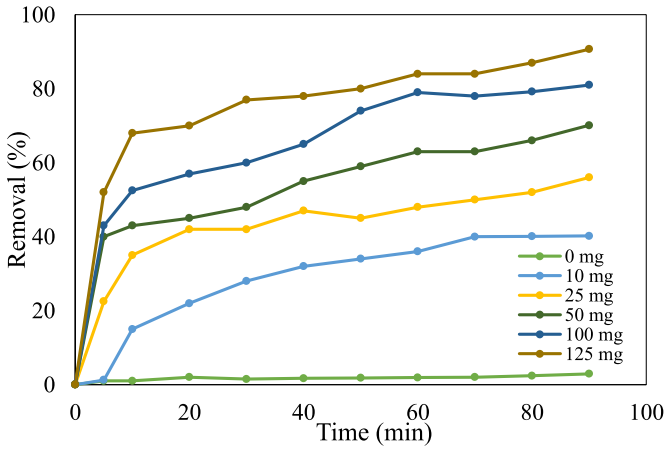

Fig. 6. The effect of catalyst loading on the photoreduction of TC using $CuInS_2$(2:1) as photocatalyst.

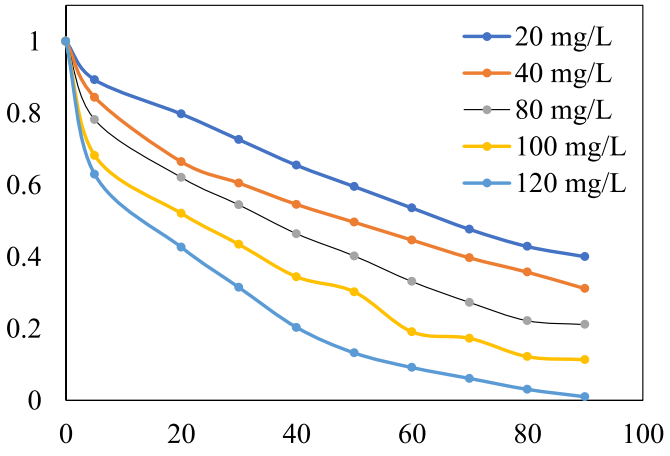

Fig. 7. (a) Effect of TC concentration on the efficiency of $CuInS_2$(2:1) (dosage: 125 mg, irradiation time: 90 min).

populate the active sites of the photocatalyst due to increased adsorption onto its surface. [47]. The reason for this is that a higher concentration of TC resulted in an inhibitive impact on the TC reaction with photogenerated hydroxyl radicals due to the reduced interaction between the two reactants [48]. The light absorption through TC molecules could also delay the photons from reaching the surface of the catalyst at a higher initial concentration of TC, thereby decreasing TC removal efficiency, similar to previous reports [49].

4. Conclusion

Copper indium sulfide ($CuInS_2$) nanoparticles were successfully synthesized by the solvothermal decomposition of two precursor complexes via the microwave irradiation method. Concentration variation of the precursor complexes afforded two different ternary nanoparticles, $CuInS_2$ (3.1) and $CuInS_2$ (2.1), which were characterized by XRD, SEM, TEM EDX, and UV-visible spectroscopy. The microscopic analysis revealed similar morphologies for both $CuInS_2$ (3.1) and $CuInS_2$ (2.1). Both ternary copper indium sulphide nanoparticles exhibited good photocatalytic efficiency of 95 and 91 % for $CuInS_2$(2:1) and $CuInS_2$(3:1), respectively. The $CuInS_2$(2:1) displayed better photocatalytic activity in the degradation of TC compared to $CuInS_2$(3:1). This was attributed to the lower band gap and higher absorption properties of the $CuInS_2$(2:1). Nevertheless, comparable degradation efficiency occurred for the $CuInS_2$(3:1) with other similar ternary photocatalysts. Therefore, both as-synthesized $CuInS_2$ could be good materials to reduce TC into a less harmful product. Our results provide valuable insight into the synthesis of ternary semiconductor nanoparticles by microwave route and the development of nanophotocatalyst for efficient tetracycline degradation, which could be extended to other organic pollutants.

Declaration of Competing Interest

The authors declare that they have no known competing financial interests or personal relationships that could have appeared to influence the work reported in this paper.

Data availability

Data will be made available on request.

Acknowledgement

The authors would like to acknowledge the North-West University, the University of South Africa (Department of Chemical Engineering, and College of Science, Engineering, and Technology), and the National Research Foundation of South Africa for financial support.

References

[1] F. Ahmad, D. Zhu, J. Sun, Environmental fate of tetracycline antibiotics: degradation pathway mechanisms, challenges, and perspectives, Environ. Sci. Europe 33 (2021) 64.
[2] B. Halling-Sørensen, G. Sengeløv, J. Tjørnelund, Toxicity of tetracyclines and tetracycline degradation products to environmentally relevant bacteria, including selected tetracycline-resistant bacteria, Arch. Environ. Contam. Toxicol 42 (2002) 263–271.
[3] S. Shao, X. Wu, Microbial degradation of tetracycline in the aquatic environment: a review, Crit. Rev. Biotechnol. 40 (2020) 1010–1018.
[4] X. He, T. Kai, P. Ding, Heterojunction photocatalysts for degradation of the tetracycline antibiotic: a review, Environ. Chem. Lett. 19 (2021) 4563–4601.
[5] J. Dai, X. Meng, Y. Zhang, Y. Huang, Effects of modification and magnetization of rice straw derived biochar on adsorption of tetracycline from water, Bioresour. Technol. 311 (2020), 123455.
[6] R. Daghrir, P. Drogui, Tetracycline antibiotics in the environment: a review, Environ. Chem. Lett. 11 (2013) 209–227.
[7] J. Chen, H. Shu, P. Niu, P. Chen, H. Jiang, Highly sensitive detection of trace tetracycline in water using a metal-organic framework-enabled sensor, Adsorpt. Sci. Technol. 2021 (2021) 1–11.
[8] D.A. Palacio, L.M. Leiton, B.F. Urbano, B.L. Rivas, Tetracycline removal by polyelectrolyte copolymers in conjunction with ultrafiltration membranes through liquid-phase polymer-based retention, Environ. Res. 182 (2020), 109014.
[9] T. Saitoh, K. Shibata, M. Hiraide, Rapid removal and photodegradation of tetracycline in water by surfactant-assisted coagulation–sedimentation method, J. Environ. Chem. Eng. 2 (2014) 1852–1858.
[10] F. Saadati, N. Keramati, M.M. Ghazi, Influence of parameters on the photocatalytic degradation of tetracycline in wastewater: a review, Crit. Rev. Environ. Sci. Technol. 46 (2016) 757–782.
[11] N. Chumha, W. Pudkon, A. Chachvalvutikul, T. Luangwanta, C. Randorn, B. Inceesungvorn, A. Ngamjarurojana, S. Kaowphong, Photocatalytic activity of CuInS2 nanoparticles synthesized via a simple and rapid microwave heating process, Mater. Res. Express 7 (2020), 015074.
[12] Y. Wang, Y. Wang, R. Xu, Synthesis of Zn–Cu–Cd sulfide nanospheres with controlled copper locations and their effects on photocatalytic activities for H2 production, Int J Hydrogen Energy 35 (2010) 5245–5253.
[13] S. Paul, S. Ghosh, D. Barman, S. De, Maximization of photocatalytic activity of Bi2S3/TiO2/Au ternary heterostructures by proper epitaxy formation and plasmonic sensitization, Appl. Catal. B 219 (2017) 287–300.
[14] O.C. Olatunde, D.C. Onwudiwe, Copper-based ternary metal sulfide nanocrystals embedded in graphene oxide as photocatalyst in water treatment. Nanotechnology in the Beverage Industry, Elsevier, 2020, pp. 51–113.
[15] J. Zhang, L. Qi, J. Ran, J. Yu, S.Z. Qiao, Ternary NiS/ZnxCd1-xS/reduced graphene oxide nanocomposites for enhanced solar photocatalytic H2-production activity, Adv Energy Mater 4 (2014), 1301925.
[16] R. Zamiri, H.A. Ahangar, D. Tobaldi, A. Rebelo, M. Seabra, M. Shabani, J. Ferreira, Fabricating and characterising ZnO–ZnS–Ag 2 S ternary nanostructures with efficient solar-light photocatalytic activity, Phys. Chem. Chem. Phys. 16 (2014) 22418–22425.
[17] C.-L. Tao, Z. Xie, D. Xu, X. Li, F. Ge, F. Chen, Z. Jiang, W. Gu, F. Cheng, X.-J. Wu, Templated synthesis of ultrathin indium-based ternary metal sulfide (MIn2S4, M= Zn, Cd, and Ni) nanoplates for photocatalytic hydrogen evolution, ACS Appl. Energy Mater. 5 (2022) 4877–4884.
[18] Y. Tian, J. Zhang, X. Yang, D. Jia, Facile one-pot synthesis and enhanced photocatalytic performances of ternary metal sulfide composite g-C3N4/Cu3SnS4, Eur. J. Inorg. Chem. 2022 (2022), e202200151.
[19] J. Zhang, A. Bifulco, P. Amato, C. Imparato, K. Qi, Copper indium sulfide quantum dots in photocatalysis, J. Colloid Interface Sci. (2023).
[20] D. Cahen, Y. Mirovsky, Ternary chalcogenide-based photoelectrochemical cells. 6. Is there a thermodynamic explanation for the output stability of copper indium sulfide (CuInS2) and copper indium selenide (CuInSe2) photoanodes? J. Phys Chem 89 (1985) 2818–2827.
[21] J. Chang, E.R. Waclawik, Controlled synthesis of CuInS 2, Cu 2 SnS 3 and Cu 2 ZnSnS 4 nano-structures: insight into the universal phase-selectivity mechanism, CrystEngComm 15 (2013) 5612–5619.
[22] R. Li, Y. Li, W. Feng, H. Wu, X. Zhong, Y. Ma, R. Xie, Facile synthesis, optical properties regulation and boosted photocatalytic degradation performance for organic pollutants of Mn: cuInS2/CdS nanocrystals, J. Lumin. 252 (2022), 119355.
[23] O. Amiri, M. Salavati-Niasari, M. Sabet, D. Ghanbari, Synthesis and characterization of CuInS2 microsphere under controlled reaction conditions and its application in low-cost solar cells, Mater. Sci. Semicond. Process 16 (2013) 1485–1494.
[24] N.B.H. Mohamed, M. Bouzidi, S. Ouni, A.S. Alshammari, Z.R. Khan, M. Gandouzi, M. Mohamed, N. Chaaben, A. Bonilla-Petriciolet, M. Haouari, Statistical physics analysis of adsorption isotherms and photocatalysis activity of MPA coated CuInS2/ZnS nanocrystals for the removal of methyl blue from wastewaters, Inorg. Chem. Commun. 144 (2022), 109933.
[25] A. Jafarinejad, H. Bashiri, M. Salavati-Niasari, Sonochemical synthesis and characterization of CuInS2 nanostructures using new sulfur precursor and their application as photocatalyst for degradation of organic pollutants under simulated sunlight, Arabian J. Chem. 15 (2022), 104007.
[26] S.S. Chetty, S. Praneetha, S. Basu, C. Sachidanandan, A.V. Murugan, Sustainable, rapid synthesis of bright-luminescent CuInS2-ZnS alloyed nanocrystals: multistage nano-xenotoxicity assessment and intravital fluorescence bioimaging in zebrafish-embryos, Sci Rep 6 (2016) 26078.
[27] H. Hao, X. Lang, Metal sulfide photocatalysis: visible-light-induced organic transformations, ChemCatChem 11 (2019) 1378–1393.
[28] N.E. Ingram, B.J. Jordan, B. Donnadieu, S.E. Creutz, Barium and titanium dithiocarbamates as precursors for colloidal nanocrystals of emerging optoelectronic materials, Dalton Trans. 50 (2021) 15978–15982.
[29] M. Sabet, M. Salavati-Niasari, D. Ghanbari, O. Amiri, Synthesis of copper indium sulfide nanoparticles via microwave approach and investigation of their behavior in solar cells, Synth. React. Inorg., Metal-Organic, and Nano-Metal Chem. 45 (2015) 1025–1032.
[30] S. Peng, J. Liang, L. Zhang, Y. Shi, J. Chen, Shape-controlled synthesis and optical characterization of chalcopyrite CuInS2 microstructures, J. Cryst. Growth 305 (2007) 99–103.
[31] B.-B. Xie, B.-B. Hu, L.-F. Jiang, G. Li, Z.-L. Du, The phase transformation of CuInS 2 from chalcopyrite to wurtzite, Nanoscale Res. Lett. 10 (2015) 1–7.
[32] M. Kruszynska, H. Borchert, J. Parisi, J. Kolny-Olesiak, Synthesis and shape control of CuInS2 nanoparticles, J. Am. Chem. Soc. 132 (2010) 15976–15986.
[33] J. Kolny-Olesiak, H. Weller, Synthesis and application of colloidal CuInS2 semiconductor nanocrystals, ACS Appl. Mater. Interfaces 5 (2013) 12221–12237.
[34] W. Wubet, D.-H. Kuo, H. Abdullah, Effects of sintering temperature and duration on the structural and electrical properties of CuBiS2 bulks, J. Solid State Chem. 230 (2015) 237–242.
[35] V. Rajendar, T. Dayakar, B. Satish, K. Subramanyam, Y. Prashanthi, Synthesis and characterization of cuins 2 nanoparticles as potential candidates for photocatalyst and photovoltaic materials, Chalcogenide Lett. 13 (2016).
[36] F. Aslan, A. Tumbul, Non-vacuum processed Cu2ZnSnS4 thin films: influence of copper precursor on structural, optical and morphological properties, J. Alloys Compd. 612 (2014) 1–4.
[37] W.A. Badawy, A review on solar cells from Si-single crystals to porous materials and quantum dots, J. Adv. Res. 6 (2015) 123–132.
[38] A. Tang, S. Qu, K. Li, Y. Hou, F. Teng, J. Cao, Y. Wang, Z. Wang, One-pot synthesis and self-assembly of colloidal copper (I) sulfide nanocrystals, Nanotechnology 21 (2010), 285602.
[39] F. Long, W.-M. Wang, H.-c. Tao, T.-k. Jia, X.-M. Li, Z.-g. Zou, Z.-y. Fu, Solvothermal synthesis, nanocrystal print and photoelectrochemical properties of CuInS2 thin film, Mater. Lett. 64 (2010) 195–198.
[40] L. Liu, H. Li, Z. Liu, Y.-H. Xie, Structure and band gap tunable CuInS2 nanocrystal synthesized by hot-injection method with altering the dose of oleylamine, Mater. Des. 149 (2018) 145–152.
[41] M. Yousefi, M. Sabet, M. Salavati-Niasari, S.M. Hosseinpour-Mashkani, Facile microwave approach for synthesis of copper–indium sulfide nanoparticles and study of their behavior in solar cell, J. Cluster Sci. 23 (2012) 491–502.
[42] H. Fakhri, A. Mahjoub, A.C. Khavar, Synthesis and characterization of ZnO/CuInS2 nanocomposite and investigation of their photocatalytic properties under visible light irradiation, Appl. Surf. Sci. 318 (2014) 65–73.
[43] F. Shen, W. Que, Y. He, Y. Yuan, X. Yin, G. Wang, Enhanced photocatalytic activity of ZnO microspheres via hybridization with CuInSe2 and CuInS2 nanocrystals, ACS Appl. Mater. Interfaces 4 (2012) 4087–4092.
[44] H. Fakhri, H. Bagheri, Highly efficient Zr-MOF@ WO3/graphene oxide photocatalyst: synthesis, characterization and photodegradation of tetracycline and malathion, Mater. Sci. Semicond. Process 107 (2020), 104815.
[45] X. Lu, W. Che, X. Hu, Y. Wang, A. Zhang, F. Deng, S. Luo, D.D. Dionysiou, The facile fabrication of novel visible-light-driven Z-scheme CuInS2/Bi2WO6 heterojunction with intimate interface contact by in situ hydrothermal growth strategy for extraordinary photocatalytic performance, Chem. Eng. J. 356 (2019) 819–829.
[46] Y. Luo, Y. Han, Y. Hua, M. Xue, S. Yu, L. Zhang, Z. Yin, X. Li, X. Ma, H. Wu, Step scheme nickel-aluminium layered double hydroxides/biochar heterostructure photocatalyst for synergistic adsorption and photodegradation of tetracycline, Chemosphere 309 (2022), 136802.
[47] F. Deng, X. Lu, Y. Luo, J. Wang, W. Che, R. Yang, X. Luo, S. Luo, D.D. Dionysiou, Novel visible-light-driven direct Z-scheme CdS/CuInS2 nanoplates for excellent photocatalytic degradation performance and highly-efficient Cr (VI) reduction, Chem. Eng. J. 361 (2019) 1451–1461.
[48] A. Turki Jalil, H. Emad Al Qurabiy, S. Hussain Dilfy, S. Oudah Meza, S. Aravindhan, M.M. Kadhim, A.M. Aljeboree, CuO/ZrO2 nanocomposites: facile synthesis, characterization and photocatalytic degradation of tetracycline antibiotic, J. Nanostruct. 11 (2021) 333–346.
[49] N. Kumar, U. Jung, B. Jung, J. Park, M. Naushad, Zinc hydroxystannate/zinc-tin oxide heterojunctions for the UVC-assisted photocatalytic degradation of methyl orange and tetracycline, Environ. Pollut. 316 (2023), 120353.